Article

A Computational Investigation of C60 Depth Profiling of Ag: Molecular Dynamics of Multiple Impact Events

Michael F. Russo Jr., Zbigniew Postawa, and Barbara J. Garrison

J. Phys. Chem. C, **2009**, 113 (8), 3270-3276• DOI: 10.1021/jp808706y • Publication Date (Web): 30 January 2009

A Computational Investigation of C_{60} Depth Profiling of Ag: Molecular Dynamics of Multiple Impact Events

Michael F. Russo, Jr.,[†] Zbigniew Postawa,[‡] and Barbara J. Garrison*[,†]

Department of Chemistry, 104 Chemistry Building, Penn State University, University Park, Pennsylvania 16802, and Smoluchowski Institute of Physics, Jagiellonian University, ul. Reymonta 4, 30-059, Kraków, Poland

Received: October 1, 2008; Revised Manuscript Received: December 16, 2008

Ⓦ **This paper contains enhanced objects available on the Internet at http://pubs.acs.org/JPCC.**

Using 20-keV C_{60} on a Ag sample, multiple cluster bombardment events have been performed with molecular dynamics simulations. The purpose of this investigation is to develop a protocol for making depth profiling simulations tractable, as well as to examine the topographical effects which arise due to multiple impacts on smooth surfaces. The results show that when the total yield is equivalent to the removal of one atomic layer (0.24 nm), the distribution of the ejected particles is spread throughout the top 5.5 nm of the sample. Examples of individual bombardment events on the damaged surface exhibit a diversity of dynamics that is not observed on flat surfaces. Using the computational methods outlined, we have been able to run depth profiling simulations on a large-scale system.

Introduction

Cluster ion beams have been paramount to the advancement of secondary ion mass spectrometry (SIMS) and its applications over the past two decades.[1,2] Their abilities of nonlinear enhancement of yield, reduced chemical damage, and reduced damage depth have opened the door to a wide array of depth profiling capabilities.[3−12] For example, it is possible to analyze multilayered structures used in the electronics/semiconductor industry,[6,13] as well as perform molecular specific depth profiles of cells and other biologically important systems.[13−20]

The critical issue for quantitative interpretation of depth profiles is the interface width, a quantity that reflects how precisely one can measure a change in composition. The depth profiling experiments utilizing C_{60} in which interface widths between similar materials such as two metals[11,12] or two Langmuir−Blodgett films[14,15] give values of 8.7 and ∼23 nm, respectively. The molecular dynamics simulations in which the depth of origin of ejected material has been investigated,[21−25] however, consistently indicate that ejected material originates from the top 2−3 nm, values much smaller than experimental interface widths. There are two essential differences from the MD simulations given above and depth profiling experiments. First, the experimental surfaces are not flat, which has been the case in the simulations. Second, the experiments are performed with multiple bombardment events at each surface position. The effect of surface topography on the bombardment event has been explored previously. Moseler et al.[26] investigated the smoothing of thin film growth due to an energetic cluster impact on "tilted" areas of the film. Also, Aoki et al.[27] utilized a Si sample with predefined, sine wave, surface features to examine the effects that concave/convex impact areas have on the sample's roughness after bombardment of several large Ar clusters. Although these types of investigations have examined the dynamics of clusters, they have been primarily performed with large clusters on the order of 10^3 to 10^6 particles. Therefore, there is still a gap between the current knowledge about a single cluster, e.g. C_{60}, and the complex interactions and environments which arise due to the multiple impacts which occur during actual experiments. Thus investigations are needed to elucidate this discrepancy and to understand these dynamics on an atomic scale, as well as to develop computational methods capable of simulating many impacts well beyond the static limit.

Using MD simulations we have investigated the topographical features that arise due to C_{60} bombardment on a Ag sample, as well as observe the effects those features have on subsequent impacts, depth resolution, and the overall yield. In this study, the sample's topography evolves "naturally" in a way analogous to what is expected to occur during experiments which use C_{60} projectile beams. A computational protocol is established that permits depth profiling calculations involving multiple impacts on a large sample to be performed. This new protocol can be used for a wide range of samples, and will allow future depth profiling simulations on more complex systems to be tractable.

Computational Details

Molecular dynamics simulations have been prevalent in a wide variety of applications involving the classical atomic motion of experimentally significant systems. The basis of the molecular dynamics procedure utilized here involves the numerical integration of Hamilton's equations of motion through time, which calculates the positions and velocities of each of the particles at each iteration step. A more detailed description of this MD scheme can be found in previously published literature.[28,29]

For the simulations described, we have created a "divide and conquer" scheme for performing several impacts simultaneously, while preserving the time dependence of the impact sequence. This procedure consists of the following steps (see Figure 1): (1) Generate a large sample to be used for the depth profiling study. This step is done by creating a small sample and then replicating it in all three dimensions to obtain the desired size, Figure 1a. (2) Using random numbers, generate a list of impact coordinates, Figure 1b. (3) Determine the size of a local sample

* Corresponding author. E-mail: bjg@psu.edu.
[†] Penn State University.
[‡] Jagiellonian University.

10.1021/jp808706y CCC: $40.75
Published on Web 01/30/2009

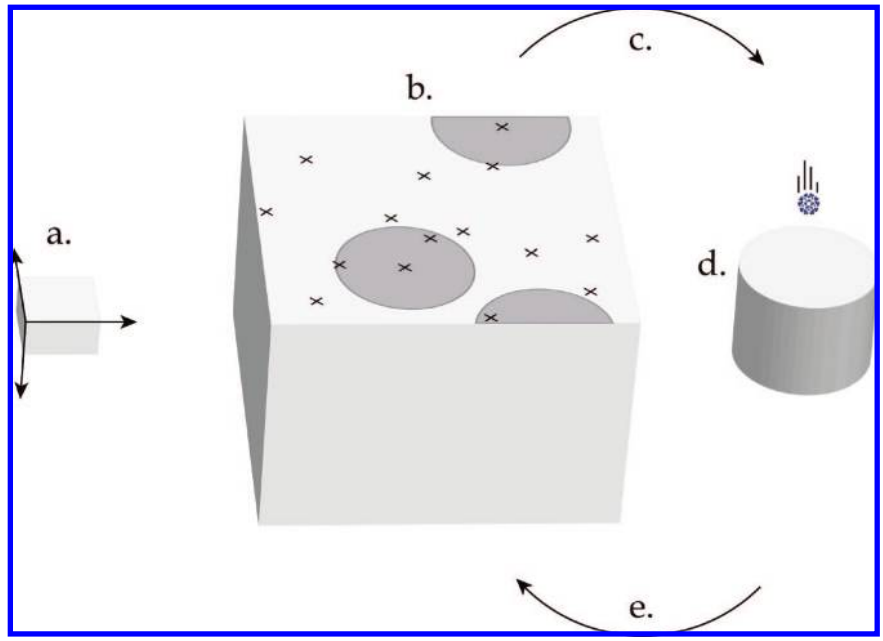

Figure 1. Schematic of the computational procedure used for multiple impacts: (a) Create a small sample to replicate. (b) Generate random impact points and determine which to run at the same time. (c) Extract particles for individual bombardments. (d) Run impacts independently. (e) After bombardment, reinsert new positions into main sample. Run the next round of impacts on the modified surface by repeating steps c through e.

that is needed to contain a single bombardment event, Figure 1c,d. (4) Choose which impacts from the list of random points can be run at the same time. The critical consideration is that the random order should not be altered. The choice of simultaneous impacts is done by using two criteria: the impact in question cannot have its local sample overlap any of the impacts already selected to be run concurrently and the impact in question cannot have its local sample overlap any of the impacts which have already been considered from the list which have been skipped thus far. (5) Copy the coordinates of all the particles within a local sample to a separate file, using periodic boundary conditions around the main sample if necessary: dark circles in Figure 1b. (6) Run a group of noninteracting impacts simultaneously as individual simulations, Figure 1d. (7) After the simulations have ended, replace the old coordinates with the new ones for each particle that was active, Figure 1e. (8) Repeat the same procedure for the next round of impacts, which will now take place on a modified surface.

The main sample used in this investigation consists of a Ag(111) crystal measuring 53 nm × 53 nm × 15 nm that contained approximately 4.5 million atoms. Each sample used for a single impact was cylindrical in shape with a radius of 10 nm and a height of 15 nm with approximately 275 000 Ag atoms. This size was chosen based on observations of the size of an impact event using C_{60} on Ag in previous simulations, ensuring that each cylinder was sufficiently large enough to contain a single event. Rigid and stochastic regions measuring 0.5 and 2.5 nm, respectively, were used on the bottom as well as cylindrically around the sides to prevent pressure waves, and maintain the shape of the sample.[30,31] These outer layers also act as a sleeve that allows for the reinsertion of the modified coordinates back into the main sample without causing particles to overlap at the edges. A 20-keV C_{60} cluster was bombarded onto each sample, normal to the original sample surface. A Moliere potential was used for the Ag−C interaction and a molecular dynamics/Monte Carlo-corrected effective medium (MD/MC-CEM) potential was used to describe the Ag−Ag interaction.[32] Due to the fact that almost all of the carbon is back-sputtered during the impacts, the small amount of embedded carbon is removed after each run and is ignored for this investigation. A total of 100 trajectories were performed, with each individual impact run for 20 ps. This amount of time was sufficient to allow the roughly 10 ps collision process to occur and then allow the sample to equilibrate. Each 20 ps simulation required approximately two days of CPU time on a 3.0 GHz Intel Xeon 3160 (Woodcrest) Dual-Core Processors.[33]

There are disparate time scales between successive impacts in the simulations and experiment. The time between successive hits at overlapping impact areas in the simulation can be as short as tens of picoseconds whereas in the experiment the time is on the order of microseconds to milliseconds depending on the ion current. On this microsecond to millisecond time scale thermal diffusion of material subsequent to the bombardment event is possible. The current MD simulations include all atomic motion to ~20 ps at which time the material is equilibrated and thus provides a starting point for possible thermal motion to occur. However, the thermal diffusion coefficient for Ag at ~560 K is 3×10^{-18} cm^2/s.[34] This small value indicates that diffusion would be at most a small contributor to interlayer mixing in this system.

Results

The first point for analyzing the results of the simulations is for a number of impacts such that an orderly arrangement would have no overlap between each crater and rim diameter. This condition approximately corresponds to the experimental static limit and for the current sample would be about 36 impacts per $(53\ nm)^2$ which corresponds to $\sim 1.3 \times 10^{12}$ impacts/cm^2. Figure 2a illustrates the main sample at the point of 36 impacts. The color scale of Figure 2a represents the height of each atom in the range from 5.5 nm below the original surface to 4.5 nm above it. It is clear that when impacting the sample at random, the nonoverlapping criterion is quickly broken. There are already several areas which have been bombarded multiple times, as well as a significant portion of the surface that is still unaffected. Figure 2b illustrates the main sample after 100 impacts. (An animation of the evolution of the topography is given as a Web-

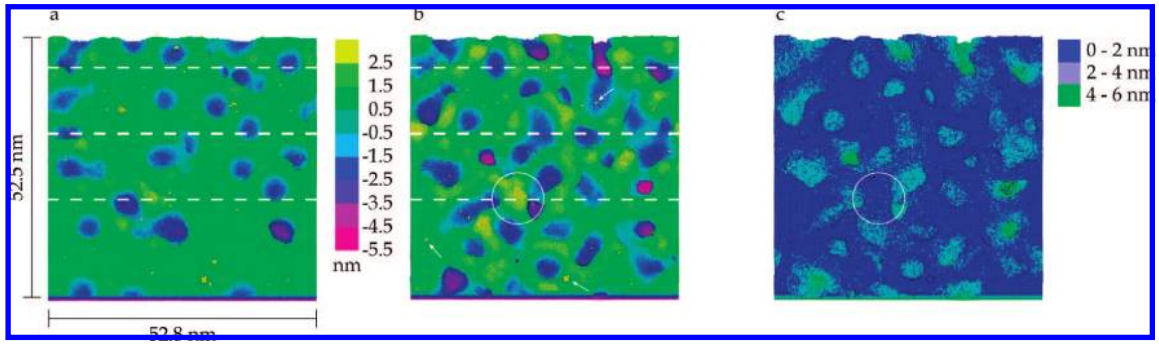

Figure 2. Topography of the entire sample: (a) Height distribution of entire sample after 36 impacts. Color scheme is based on height position of the material from a depth of 5.5 nm below the original sample to 4.5 nm above. (b) Image of the sample after 100 impacts. The circled area indicates a mountain that has formed. Arrows indicate some examples of material floating above the surface. (c) Ag atoms of the main sample colored according to their original depths before any impacts have occurred. Coloring is divided into layers measuring 2 nm thick. Circled area shows the mountain from 2b is comprised of material from the top two nanometers of the sample. (An animation of part b is available as a Web-enhanced object.)

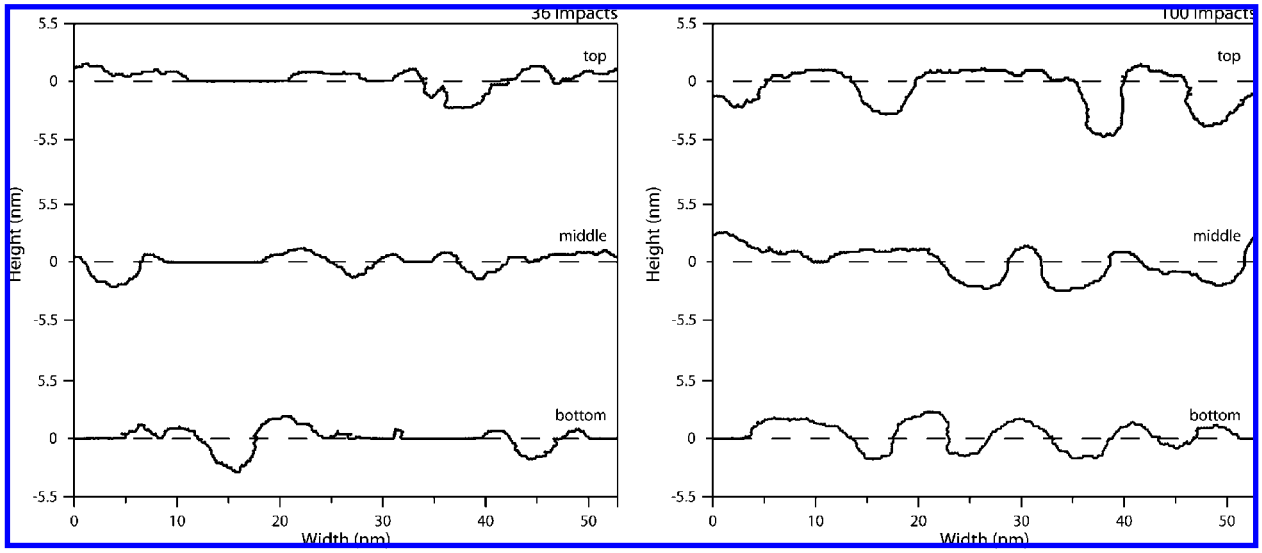

Figure 3. Three representative line scans of the surface topography at 36 and 100 impacts. Each line corresponds to the dashed lines shown in Figure 2, parts a and b.

enhanced object.) From Figure 2b the various types of topographical environments that develop are evident. Several areas have been hit multiple times with close proximity, forming large mound structures, while others have formed elongated ditches as a result of adjacent impacts. Of interest is the relatively shallow depth of the damage, approximately 5 nm, even for those areas which have been impacted several times. This shallow depth is due to a large amount of lateral motion associated with each impact. This lateral motion is evident from Figure 2c, in which the coloring represents 2-nm layers of material based on their original positions at time equal to zero. The mound structures which appear yellow in Figure 2b are approximately 3 nm above the original surface (circled), and are comprised almost completely of material from the first 2 nm (blue atoms in 2c) of the sample. Figure 3 depicts three examples of the topographical evolution from 36 to 100 impacts. These profiles are taken across the sample, as shown by the three dashed lines in Figure 2a,b. Line a and line b were chosen to illustrate the lowest and highest features, respectively. For 36 impacts, the large amount of surface that has not been altered yet is evident. Only small craters and rims are present as well. Conversely for 100 impacts, there are almost no unaffected surface regions. Several of the small features initially present have now been eroded or filled in.

As discussed above, one of the goals of this investigation is to bridge the gap between the experimental interface widths[12,14] and the seemingly conflicting computational picture. In particular, how do such large interface widths occur when the depth of the craters created during simulations of a C_{60} impact is on the order of 2 to 3 nm deep? Each single impact event, however, deposits some sample material from the crater region to the rim and some material from directly below the impact point is driven into the bottom of the crater. This upward and downward motion of sample material will affect the ultimate depth resolution. The accumulation of the removal of material and upward/downward motion is summarized in Figure 4, in which the yield for the entire system over the course of all 100 impacts is represented. Each set of data depicts the fraction of removal from regions comprised of two original crystal layers. At 100 impacts a total of 39 294 Ag particles have been removed from the entire sample. This amount is roughly equal to the number of particles that make up one monolayer of the main sample (38 430 Ag particles/layer). Examining the yield for the two topmost layers (0−0.35 nm) of the sample in Figure 4, however, indicates that only slightly more than 20% of the material in these layers has been removed. At the same time, sputtering of material as deep as 5 to 6 nm deep is observed in Figures 2 and 3. (Only depths of 12 layer/2.7 nm are shown in Figure 4 for clarity.) From

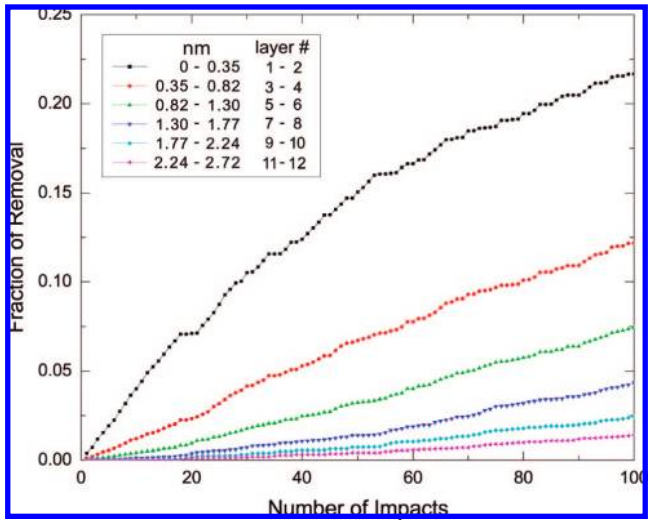

Figure 4. Fraction of material sputtered from various strata within the sample. Each group corresponds to two horizontal crystal layers.

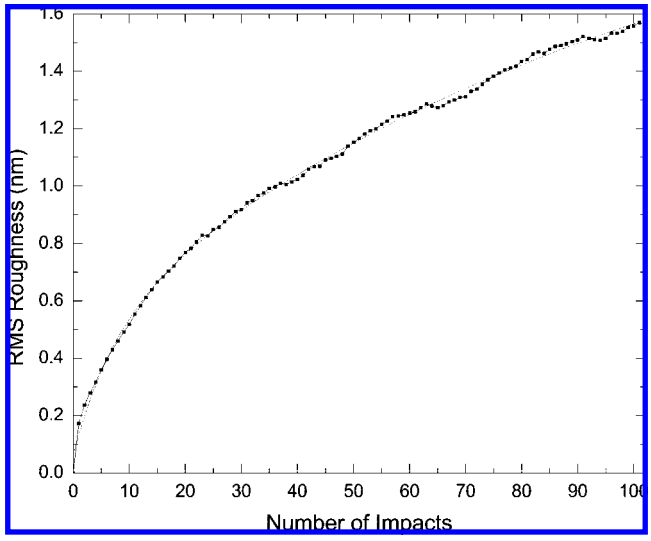

Figure 5. Root-mean-square roughness in nanometers of the entire sample versus the number of C_{60} impacts. The fit-line is generated from a two-phase exponential association curve given by the following equation: $y = y_0 + A_1(1 - e^{(-x/t_1)}) + A_2(1 - e^{(-x/t_2)})$, where $y_0 = 0.064$ nm, $A_1 = 0.424$ nm, $A_2 = 1.775$ nm, $t_1 = 7.4$ impacts, and $t_2 = 107$ impacts. This equation gives a final roughness value of 2.3 nm.

this information, it is feasible to imagine that the distribution of the sputtered material's original depth will be even deeper by the time the top two layers have reached a value of over 90% removed. In comparison to experiments with metal samples, Sun et al. previously determined the interface width between the two constituents of the Ni:Cr sample to be approximately 8.7 nm in thickness for an incident energy of 20 keV.[11] This value is consistent with the result from this simulation giving that about 8−9 nm of topography has been created in removing only 0.24 nm of material as shown in Figures 2 and 3. Thus crater depths calculated for single impacts on flat surfaces are not appropriate for experimental interface widths.

The root-mean-square (rms) roughness of the entire sample as a function of the number of impacts is shown in Figure 5. To calculate the rms roughness, the sample was discretized into 0.4 nm by 0.4 nm columns, with each column giving a surface height value. This size was chosen in order to be as small as possible for accuracy, but large enough so as not to obtain

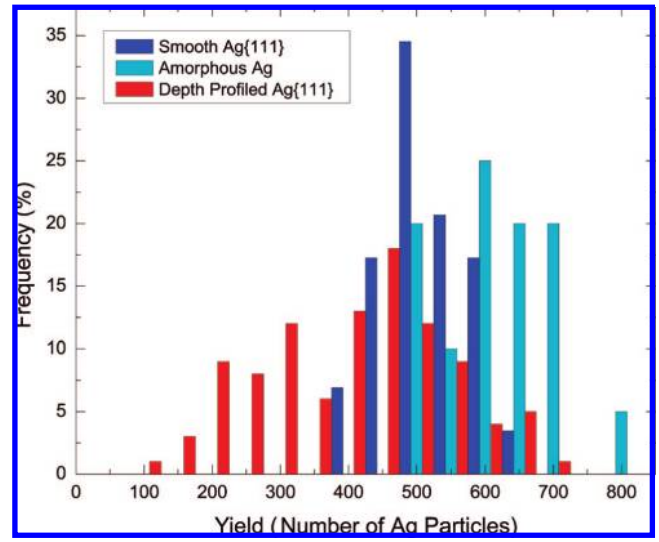

Figure 6. Frequency of yield totals observed after 20-keV C_{60} events on Ag for the depth profiling simulations (red), flat crystalline Ag (blue), and flat amorphous Ag (cyan) samples. Yields have been separated into bins of 50 particles. No interaction between impacts occurred for the flat crystalline or flat amorphous samples. Each impact took place on a pristine sample, with different impact points.

measurements of zero between crystal lattice rows. After 100 impacts, the roughness has reached a value of approximately 1.5 nm. We fit a two-phase associative exponential curve to these data (shown in Figure 5) to examine the roughness trend. This type of curve consists of a fast and slow exponential decay, which in this case has a half-life of 5 and 70 impacts, respectively. We attribute the initial fast decay to the fact that the roughness of the sample is rapidly changing due to the flat surface starting conditions. This phase then moves into the more natural, slow decay caused by multiple bombardments. With this trendline, the estimated final roughness value is 2.3 nm. Observing the graph, however, we feel it is still too early to determine an exact value, and an order of magnitude more impacts might be necessary.

A comparison of the yields for the entire system versus yields on smooth Ag surfaces is shown in Figure 6. The blue data points represent the normalized results of 29 individual trajectories of 20-keV C_{60} on a Ag(111) sample. Each trajectory was run with the cluster impact taking place normal to the surface, but at a slightly different point at the surface, in order to study the crystallographic effects on the yield. The cyan data represent the same information as the blue, with the exception that it is normalized data obtained over 20 different impacts on a smooth, amorphous Ag sample. The mean value of these amorphous impacts is slightly larger, 492 sputtered Ag particles for the crystalline versus 591 Ag particles for the amorphous sample. The single-crystal structure allows the energy of the cluster to dissipate more quickly than that of the amorphous sample. When comparing these sets of data to the current results (red data points), it is evident that the roughening of the surface has caused the yield distribution to become broader, as well as shifted toward a lower average of 377 sputtered Ag particles. To understand this trend, we have examined the various ways in which the local roughness conditions can affect the yield of impact events.

We have investigated the various types of local environments which are produced by multiple impacts, and how these environments affect the trend of changing roughness. For our analysis, the local roughness of each impact point was calculated

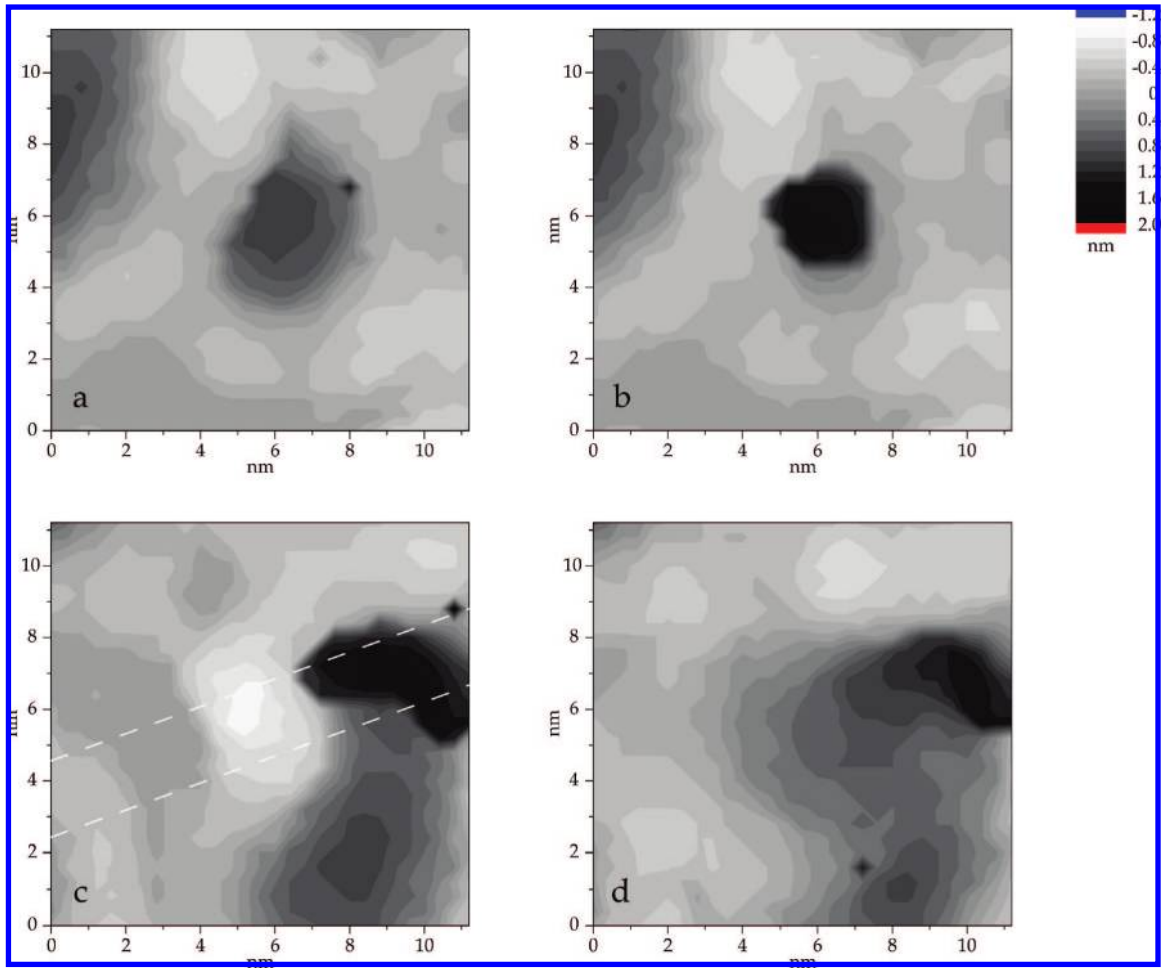

Figure 7. Before and after surface topologies of impacts which exhibit significant roughness change. In each case, the impact was at the center of the sample shown in the figure. (a, b) Before and after images for an impact on a concave crater area. (c, d) Before and after images for an impact on a convex mound area. Dotted lines on part c represent the 20°, 2 nm thick slice used in the figure.

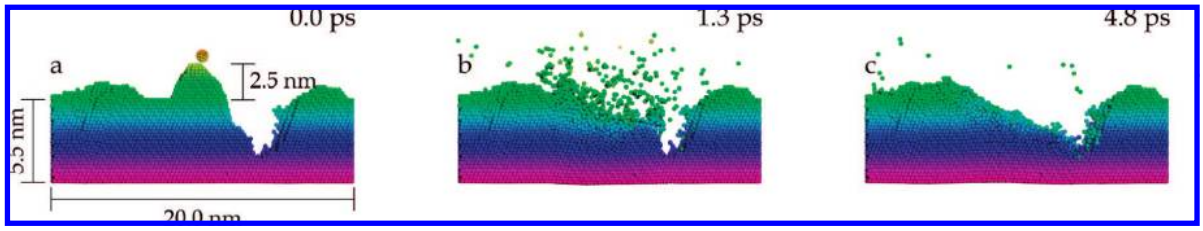

Figure 8. Snapshots of a smoothing impact on a mound structure. Images are composed of slices which are 2 nm thick, taken along a 20° cut of the sample (see Figure 4). (a) Time equals zero showing the mound below the C_{60} projectile. (b) After 1.3 ps showing the mound has exploded as well as material beginning to fill in the adjacent crater. (c) After approximately 5 ps the entire mound is removed as well as a significant portion of the crater. (An animation is available as a Web-enhanced object.)

both before and after the bombardment to determine the change caused. Figure 7 illustrates examples of impacts which exhibit a typical increase (a, b) and decrease (c, d) of roughness. The defining topographical feature that produces an increase in the roughness is an impact that occurs within a depression or preexisting crater. This behavior is evident in Figure 7a,b where after the impact, the preexisting crater has been made deeper while the surrounding material has been almost completely unharmed. Conversely, an impact at the convex structures produces a decrease in roughness. In Figure 7c,d we see a mound structure directly below the impact point that is completely destroyed after bombardment. Again, much of the surrounding area is unaffected while the feature is completely removed. In Figure 8, we have taken a slice of Figure 7c (marked by the dashed lines), which includes a profile of both the mound and the nearby crater, to get a more detailed look at this behavior (see the Web for full animation of this bombardment). Here we can see three snapshots during the bombardment of the mound structure illustrated in Figure 7c,d. The color scheme is based on the height of each atom at time equals zero for this impact event. Only material from a range of 4.5 nm above to 5.5 nm below the original surface is shown for image simplicity. During the course of the C_{60} impact, the entire 2.5 nm high mound is destroyed. Because there is no bulk material surrounding it, the mound particles are ejected outward from the impact in all directions where the vacuum is present. Some of this material is sputtered; however, the majority of the particles contact the surface and the adjacent crater wall; effectively filling in the crater. Similar trends have been observed by other researchers. Aoki et al. observed the same dynamics

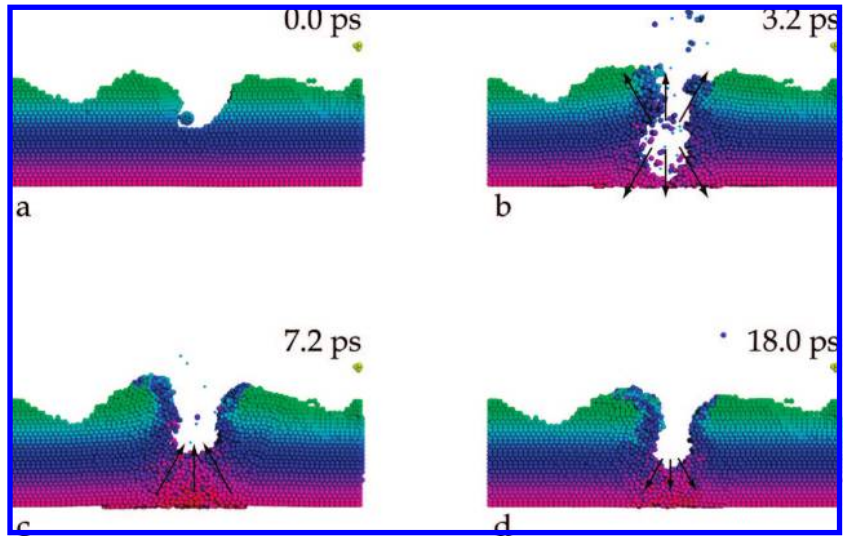

Figure 9. Snapshots of a roughness increasing impact on a concave surface feature. Images are of a 2 nm slice cut horizontally from the impact in Figure 3a,b. (a) The impact point for the C_{60} is directly at the bottom of the crater. (b) After ~3 ps the crater is twice its original depth. (c) Swelling of the bulk material toward the vacuum of the crater region. (d) Relaxation of crater region. (An animation is available as a Web-enhanced object.)

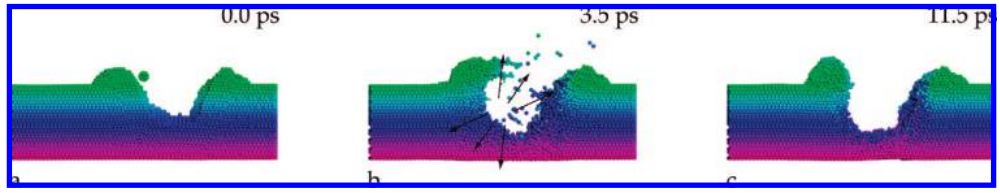

Figure 10. Snapshots of an impact on the sidewall of a preexisting crater. Images are of a 2 nm slice centered at the point of impact. (a) Position of the C_{60} projectile before impact of the crater. (b) Material is energized and travels outward from the point of impact. Dark blue material from the bottom of the crater is now redeposited on the opposing sidewall. (c) The crater has been expanded and deepened by the impact. (An animation is available as a Web-enhanced object.)

with large Ar cluster bombardment of Si.[27] Also, a similar "downward current" as in previous research performed by Moseler et al. can be seen with raised material flowing down to fill in the depressions nearby.[26]

As discussed above, these types of bombardments on mounds of surface material cause particles to be accelerated in all directions in which the vacuum is present for them to move into. This behavior means that there can be a subset of material that travels radially out from the point of impact, and parallel or near-parallel to the surface. Without neighboring surface features of a significant height, these particles have the ability to travel a fairly large distance. Some examples of such particles and clusters are evident in Figure 2b as small bright yellow "anomalies". In the current discussion, we cannot offer a hypothesis as to the experimental impact/importance of these particles, and further studies are needed in order to shed light on this phenomenon.

The dynamics of a concave, roughness increasing, impact are illustrated in Figure 9. These slices are created in the same manner as described above for Figure 8, with the exception that they are taken directly across (horizontal) the sample described in Figure 7a,b (see the Web for full animation of this bombardment). Initially we see (Figure 9a) that the C_{60} is set to impact directly at the bottom of the crater. The close proximity of the impact to the left side of the crater is an illusion of the viewing angle. After a few picoseconds (Figure 9b), there is the radial expansion of energetic material from below the impact point as indicated by the arrows. This expansion is typical of cluster bombardment as was discussed in previous works.[22,35] In this case, however, the high walls block the ejecting material from escaping into the vacuum, only allowing sputtering of material from a small window of angles off normal to the surface. The majority of this material collects on the walls of the crater as is evident from the amount of deep blue particles present on the crater sides in Figure 9c. Also from Figure 9c, there is a large upheaval of bulk material toward the vacuum of the crater as indicated by the arrows. It is hypothesized that this behavior is due to the fact that the preexisting crater did not allow the current impact to form its normal, hemispherical shaped crater. Thus the compression of material due to the initial impact is reflected back and focused at the center of the current crater, causing a vertical surge. Finally, after a long equilibration, the material settles into the shape of a long, narrow crater, which has approximately half the width of the original surface feature, and is 4−6 crystal layers deeper.

To illustrate the dynamics of an intermediate impact between the two previously discussed cases, an examination of an impact on the sloping sidewall of a crater is shown in Figure 10 (see the Web for full animation of this bombardment). During the initial contact with the surface, the C_{60} projectile shatters as the individual carbon atoms continue to cascade downward. Material is energized and begins to lift off of the tilted surface primarily at angles normal to the surface, and complimentary to the incident angle of impact. This behavior causes redeposition of material along the bottom of the crater, as well as on the opposing sidewall. In addition, the hole that is created in the side of the preexisting crater creates a lip/overhang above it that blocks the sputtering of material out into the vacuum. The end result is a crater that has been made deeper by 4−6

layers as with the concave example, and wider as a result of the peeling back of the original rim.

Conclusions

We have developed a computational method for managing multiple impact simulations of large-scale systems. Using a "divide and conquer" scheme, we are able to run multiple impacts independently, reinserting the resulting positions into the main sample. This protocol allows us to perform depth profiling simulations which retain the time dependent nature of the interactions between impacts. This method should allow for other depth profiling simulations of more complex samples to be performed in a tractable time frame.

The MD simulations which have been discussed here provide insight into the topographical features which can arise during depth profiling experiments. We have examined the interaction of multiple cluster impacts on a surface and the topography that forms as a result of those impacts. After 100 impacts, the equivalence of one crystal layer has been removed from the sample. Examining the depth of origin distribution of the sputtered material has revealed that only ~20% of the top two surface layers have been removed, with material being removed from a maximum depth of 5−6 nm. This distribution is an indication that the length scale of the interface width will be a minimum of a few to tens of nanometers deep as is observed in experiment, rather than the 2 to 3 nm depicted from a single C_{60} bombardment event. A comparison of the yield distribution to that of a flat crystalline and flat amorphous sample indicates that the topographical complexities which arise from the interaction of multiple impact events cause both a decrease in the average yield and a broadening of the range of yields observed. These simulations have shown an increase in the surface rms roughness, from 0 to approximately 1.5 nm, as a result of the surface features created via the interactions of randomly selected impacts.

Investigating the various features a C_{60} cluster can encounter, the ideal cases for a roughness increase and decrease are bombardment of a convex and concave surface feature, respectively. We have demonstrated that there is a wide variation in the dynamics which occur for bombardments of these different types of surface geometries. During bombardment of a mound feature, material is thrown out from the point of impact in all directions. Much of this material is sent outward at angles that are perpendicular to the original surface normal or greater as a result of the initial velocity of the projectile. This motion means that the majority of this material gets redeposited on the surface or travels near the surface until it impacts a secondary feature (adding to mountain growth or the filling in of a crater). For an impact in a preexisting crater, the sputtering of material is restricted by the sides of the crater, as well as the material that is adhering to the walls during the impact process, as described above. Intermediate impacts, which take place along the tilted sides of a preexisting crater, exhibit a similar reduction in sputtering efficiency. The primary angle for material to lift off and travel is downward along the slope of the tilted surface and normal to the tilted surface, impacting the other side of the crater.

Acknowledgment. The authors would like to thank the Chemistry Division of the National Science Foundation grant no. CHE-0456514 and the Polish Ministry of Science and Higher Education programs no. PB 4097/H03/2007/33 and N N204 093535 for their financial support of this research. The authors would also like to thank the Pennsylvania State University High Performance Computing Group for use of their computing resources and technical support.

References and Notes

(1) Castner, D. G. *Nature* **2003**, *422*, 129.
(2) Winograd, N. *Anal. Chem.* **2005**, *77*, 142A.
(3) Mahoney, C. M.; Fahey, A. J.; Gillen, G. *Anal. Chem.* **2007**, *79*, 828.
(4) Mahoney, C. M.; Fahey, A. J.; Gillen, G.; Xu, C.; Batteas, J. D. *Anal. Chem.* **2007**, *79*, 837.
(5) Kim, K. J.; Simons, D.; Gillen, G. *Appl. Surf. Sci.* **2007**, *253*, 6000.
(6) Gillen, G.; Batteas, J.; Michaels, C. A.; Chi, P.; Small, J.; Windsor, E.; Fahey, A.; Verkouteren, J.; Kim, K. J. *Appl. Surf. Sci.* **2006**, *252*, 6521.
(7) Cheng, J.; Wucher, A.; Winograd, N. *J. Phys. Chem. B* **2006**, *110*, 8329.
(8) Gillen, G.; Fahey, A.; Wagner, M.; Mahoney, C. *Appl. Surf. Sci.* **2006**, *252*, 6537.
(9) Wucher, A.; Cheng, J.; Winograd, N. *Anal. Chem.* **2007**, *79*, 5529.
(10) Cheng, J.; Kozole, J.; Hengstebeck, R.; Winograd, N. *J. Am. Soc. Mass Spectrom.* **2007**, *18*, 406.
(11) Sun, S.; Szakal, C.; Roll, T.; Mazarov, P.; Wucher, A.; Winograd, N. *Surf. Interface Anal.* **2004**, *36*, 1367.
(12) Sun, S.; Wucher, A.; Szakal, C.; Winograd, N. *Appl. Phys. Lett.* **2004**, *84*, 5177.
(13) Jones, E. A.; Lockyer, N. P.; Vickerman, J. C. *Anal. Chem.* **2008**, *80*, 2125.
(14) Zheng, L. L.; Wucher, A.; Winograd, N. *J. Am. Soc. Mass Spectrom.* **2008**, *19*, 96.
(15) Zheng, L. L.; Wucher, A.; Winograd, N. *Appl. Surf. Sci.* **2008**, *255*, 816.
(16) Shard, A. G.; Brewer, P. J.; Green, F. M.; Gilmore, I. S. *Surf. Interface Anal.* **2007**, *39*, 294.
(17) Shard, A. G.; Green, F. M.; Brewer, P. J.; Seah, M. P.; Gilmore, I. S. *J. Phys. Chem. B* **2008**, *112*, 2596.
(18) Fletcher, J. S.; Conlan, X. A.; Lockyer, N. P.; Vickerman, J. C. *Appl. Surf. Sci.* **2006**, *252*, 6513.
(19) Fletcher, J. S.; Lockyer, N. P.; Vaidyanathan, S.; Vickerman, J. C. *Anal. Chem.* **2007**, *79*, 2199.
(20) Cheng, J.; Winograd, N. *Anal. Chem.* **2005**, *77*, 3651.
(21) Postawa, Z.; Czerwinski, B.; Szewczyk, M.; Smiley, E. J.; Winograd, N.; Garrison, B. J. *J. Phys. Chem. B* **2004**, *108*, 7831.
(22) Russo, M. F., Jr.; Garrison, B. J. *Anal. Chem.* **2006**, *78*, 7206.
(23) Krantzman, K. D.; Webb, R. P.; Garrison, B. J. *Appl. Surf. Sci.* **2008**, *255*, 837.
(24) Ryan, K. E.; Garrison, B. J. *Anal. Chem.* **2008**, *80*, 6666.
(25) Postawa, Z.; Czerwinski, B.; Winograd, N.; Garrison, B. J. *J. Phys. Chem. B* **2005**, *109*, 11973.
(26) Moseler, M.; Rattunde, O.; Nordiek, J.; Haberland, H. *Nucl. Instrum. Methods Phys. Res., Sect. B* **2000**, *164*, 522.
(27) Aoki, T.; Matsuo, J.; Yamada, I. *Mater. Res. Soc. Symp. Proc.* **2004**, 792.
(28) Garrison, B. J. *Chem. Soc. Rev.* **1992**, *21*, 155.
(29) Garrison, B. J. Molecular Dynamics Simulations, the Theoretical Partner to Static SIMS Experiments In *ToF-SIMS: Surface Analysis by Mass Spectrometry*; Vickerman, J. C., Briggs, D., Eds.; Surface Spectra: Manchester, 2001; p 223.
(30) Postawa, Z.; Czerwinski, B.; Szewczyk, M.; Smiley, E. J.; Winograd, N.; Garrison, B. J. *Anal. Chem.* **2003**, *75*, 4402.
(31) Moseler, M.; Nordiek, J.; Haberland, H. *Phys. Rev. B* **1997**, *56*, 15439.
(32) Kelchner, C. L.; Halstead, D. M.; Perkins, L. S.; Wallace, N. M.; Depristo, A. E. *Surf. Sci.* **1994**, *310*, 425.
(33) Pennsylvania State University High Performance Computing Group: http://gears.aset.psu.edu/hpc/systems/lionxc/, 2008.
(34) Lam, N. Q.; Rothman, S. J.; Mehrer, H.; Nowicki, L. J. *Phys. Status Solidi B* **2006**, *57*, 225.
(35) Russo, M. F., Jr.; Szakal, C.; Kozole, J.; Winograd, N.; Garrison, B. J. *Anal. Chem.* **2007**, *79*, 4493.

JP808706Y